

Dependence of direct neutron capture on nuclear-structure models

T. Rauscher

Institut für Physik, Universität Basel, Klingelbergstr.82, CH-4056 Basel, Switzerland

R. Bieber, H. Oberhummer

Institut für Kernphysik, Technische Universität Wien, Wiedner Hauptstr. 8-10, A-1040 Wien (Vienna), Austria

K.-L. Kratz

Institut für Kernchemie, Universität Mainz, Fritz-Strassmann-Weg 2, D-55099 Mainz, Germany

J. Dobaczewski

Institute of Theoretical Physics, Warsaw University, Hoża 69, PL-00681 Warsaw, Poland

P. Möller*

Institut für Kernchemie, Universität Mainz, Fritz-Strassmann-Weg 2, D-55099 Mainz, Germany

M.M. Sharma

Physics Department, Kuwait University, Kuwait 13060

Abstract

The prediction of cross sections for nuclei far off stability is crucial in the field of nuclear astrophysics. We calculate direct neutron capture on the even-even isotopes $^{124-145}\text{Sn}$ and $^{208-238}\text{Pb}$ with energy levels, masses, and nuclear density distributions taken from different nuclear-structure models. The utilized structure models are a Hartree-Fock-Bogoliubov model, a relativistic mean field theory, and a macroscopic-microscopic model based on the finite-range droplet model and a folded-Yukawa single-particle potential. Due to the differences in the resulting neutron separation and level energies, the investigated models yield capture cross sections sometimes differing by orders

*Permanent address: P. Moller Scientific Computing and Graphics, Inc., P.O. Box 1440, Los Alamos, NM 87544

of magnitude. This may also lead to differences in the predicted astrophysical r-process paths.

I. INTRODUCTION

Explosive nuclear burning in astrophysical environments produces unstable nuclei which again can be targets for subsequent reactions. Most of these nuclei are not accessible in terrestrial laboratories or not fully explored by experiments, yet.

Approximately half of all stable nuclei observed in nature in the heavy element region $A > 60$ were produced in the so-called r-process (i.e., rapid neutron capture process), which is believed to occur in type II supernova explosions (see e.g., [1,2]). An environment with a high neutron density is the prerequisite for such an r-process, in which heavier elements are built up from seed elements by consecutive neutron captures and β -decays. Because of the abundant neutrons, a multitude of neutron captures ($\simeq 15 - 35$) may occur until the β -decay half-life becomes shorter than the half-life against neutron capture. Thus, the r-process path along which reactions take place, is pushed off the region of stability towards neutron-rich unstable nuclei. The location of the path has consequences for the resulting nuclear abundances, calculated in astrophysical models [3,4].

For most of the required neutron capture cross sections the statistical model (compound nucleus (CN) mechanism, Hauser-Feshbach approach) can be applied. This model employs a statistical average over resonances, for which one has to know level densities but not necessarily exact excitation energies and level spin assignments. However, the criterion for the applicability of that model is a sufficiently high level density. Especially for some light nuclei it has been known for years that the statistical model cannot be applied and that the direct capture (DC) mechanism dominates the cross sections. Nevertheless, it has only been realized recently that also for intermediate and heavy nuclei the direct mechanism can become important near shell closures and for neutron-rich isotopes when the level density becomes too low for the CN mechanism. When approaching the drip-line, neutron separation energies decrease and the nuclei become less deformed, both leading to a smaller level density at the relevant projectile energy. This relevant energy is determined by the peak $E = kT$ of the Maxwell-Boltzmann velocity distribution of the neutron gas. If a segment of the r-process path at a given element lies close enough to the drip-line, the statistical model will not be applicable anymore and the DC reactions will dominate [5,6].

The relation between DC and CN mechanisms has already been studied for neutron capture by light and intermediate target nuclei [2,7–12]. Investigations of the dependence of the level density on charge and mass number and a discussion of the applicability of the statistical model have been given elsewhere [13]. In this paper we want to investigate direct neutron capture on neutron-rich Sn and Pb isotopes with the emphasis on discussing the difficulties, the level of reliability as well as the predictive power of theoretical calculations.

The main problem for the DC predictions is that neutron separation energies and level properties (excitation energies, spins, parities) have to be known accurately, contrary to a statistical calculation in which it is sufficient to know the level density. As in the foreseeable future one can not expect any experimental information for the majority of nuclei close to the drip-line, one has to turn to theory for providing the input for the DC calculations. At the moment, there are several microscopic and macroscopic-microscopic descriptions competing in the quest for predicting nuclear properties far off stability. For the first time, in this work we want to investigate the difference in the level structure between several models and its impact on predicted neutron capture cross sections. The compared models are a

Hartree-Fock-Bogoliubov (HFB) model with the Skyrme SkP force [14,15], a relativistic mean field theory (RMFT) with the parameter set NLSH [16,17], and the macroscopic-microscopic finite-range droplet model FRDM (1992) which was also used in calculations of nuclear ground-state masses and deformations [18,19] and in calculations of quantities of astrophysical interest [20].

In Section II we very briefly introduce the method of the DC calculation and Section III gives an overview of the utilized microscopic models. For ^{208}Pb , the DC results can directly be compared to experimental values. This is described in Section IV. In the following Sections V and VI we present our results for the heavy Pb and Sn isotopes. Possible astrophysical signatures and remaining uncertainties are discussed in Section VII. The paper is concluded by the summary section VIII.

II. DIRECT CAPTURE AND FOLDING PROCEDURE

The theoretical cross section σ^{th} is derived from the DC cross section σ^{DC} given by [12,21]

$$\sigma^{\text{th}} = \sum_i C_i^2 S_i \sigma_i^{\text{DC}} \quad . \quad (1)$$

The sum extends over all possible final states (ground state and excited states) in the residual nucleus. The isospin Clebsch-Gordan coefficients and spectroscopic factors are denoted by C_i and S_i , respectively. The DC cross sections σ_i^{DC} are essentially determined by the overlap of the scattering wave function in the entrance channel, the bound-state wave function in the exit channel, and the multipole transition operator. For the computation of the DC cross section we used the direct capture code TEDCA [22], which includes E1, M1 and E2 transitions.

For determining the nucleon-nucleus potential the folding procedure was employed, a method already successfully applied in the description of many systems. In this approach the nuclear target density ρ_{T} is folded with an energy and density dependent nucleon-nucleon interaction v_{eff} [23]:

$$V(R) = \lambda V_{\text{F}}(R) = \lambda \int \rho_{\text{T}}(\mathbf{r}) v_{\text{eff}}(E, \rho_{\text{T}}, |\mathbf{R} - \mathbf{r}|) d\mathbf{r} \quad , \quad (2)$$

with \mathbf{R} being the separation of the centers of mass of the two colliding nuclei. The normalization factor λ accounts for effects of antisymmetrization and is close to unity. The nuclear density ρ_{T} can be derived from experimental charge distributions or from theory. The potential obtained in this way ensures the correct behavior of the wave functions in the nuclear exterior. At the low energies considered in astrophysical events the imaginary parts of the optical potentials are small.

In connection with the results presented below it is useful to recapitulate the sensitivity of the DC calculations to various elements of the description. In ascending importance, in the present context the DC is sensitive to the optical potential and density distribution, respectively, the reaction Q -value, and the spin and parity of a level.

For the accuracy attempted here, there is almost no difference in the results obtained by employing the optical potentials derived from the density distributions of the different models while leaving all other properties unchanged.

A stronger dependence is seen when examining changes in the Q -value. An increase in the Q -value will give a non-linear increase in the resulting cross section. As the Q -value is computed as the difference in the binding energies of target and residual nucleus (i.e., the neutron separation energy) minus the excitation energy of the level into which the neutron is captured

$$Q_i = (B_T - B_R) - E_i = S_n - E_i \quad , \quad (3)$$

the cross section will be sensitive to the masses (separation energies) derived in the different microscopic models as well as the level structure (excitation energies) given in these models.

The by far strongest sensitivity is that to spins and parities of the involved initial and final states. In order to comply with the electromagnetic selection rules, a state has to have the proper parity to contribute to the cross section significantly. The dominant contribution to the DC cross section will stem from an E1 transition. In this case, parity has to change. Consequently, the capture of an incoming neutron p -wave will be important for the Pb isotopes, whereas s -wave capture is dominating in the Sn cases. Furthermore, significant contributions only arise from low spin states like 1/2 and 3/2 states, whereas the capture to levels with higher spins is strongly suppressed. In this respect, it will prove to be important that the different microscopic models make different predictions on which states are neutron-bound and which are not, since DC can only populate bound states.

III. THE MICROSCOPIC INPUT

The energy levels, masses, and nuclear density distributions needed as input for the DC calculation were taken from three different approaches. The first one was the RMFT which has turned out to be a successful tool for the description of many nuclear properties [24]. The RMFT describes the nucleus as a system of Dirac nucleons interacting via various meson fields. There are six parameters which are usually obtained by fits to finite nuclear properties. For our calculations we have used the parameter set NLSH [16,17].

The second method was FRDM (1992), which is a macroscopic-microscopic model based on the finite-range droplet macroscopic model and a folded-Yukawa single-particle potential [18]. For pairing, the Lipkin-Nogami pairing model [25] is employed. This model proved to be very successful in reproducing ground state spins along magic numbers [26] and has been used in QRPA calculations of β -decay half lives [26,20] and for nuclear mass determinations [19].

Finally, we also utilized the self-consistent mean field HFB model [14,15] in which the nuclear states are calculated by a one-step variational procedure minimizing the total energy with respect to the occupation factors and the single-particle wave functions simultaneously.

To be able to compare the predictions from all of the models the nuclei were considered to be spherically symmetric. The limitations of such a restriction are discussed in Section VII.

IV. COMPARISON WITH EXPERIMENTS FOR THE $^{208}\text{Pb}(n,\gamma)^{209}\text{Pb}$ REACTION

Recently, it became possible to extract the non-resonant part of the experimental capture cross section for the $^{208}\text{Pb}(n,\gamma)^{209}\text{Pb}$ reaction [27]. In that work, high resolution neutron capture measurements were carried out in order to determine twelve resonances in the range 1–400 keV. From these values the resonant Maxwellian-averaged cross section $\langle \sigma \rangle_{30\text{keV}}^{\text{R}} = 0.221(27)$ mb was calculated. Measurements of the total cross section using neutron activation [28,29] are also available at 30 keV, yielding the value $\langle \sigma \rangle_{30\text{keV}}^{\text{t}} = 0.36(3)$ mb. By a simple subtraction of the resonant part from the total cross section the value of $\langle \sigma \rangle_{30\text{keV}}^{\text{NR}} = 0.14(4)$ mb can be deduced for the non-resonant capture cross section.

Using the experimentally known density distributions [30], masses [31] and energy levels [32], we calculated the non-resonant contribution in the DC model. The strength parameter λ of the folding potential in the neutron channel was fitted to experimental scattering data at low energies [33]. The value of λ for the bound state is fixed by the requirement of correct reproduction of the binding energies. The spectroscopic factors for the relevant low lying states of ^{209}Pb are close to unity as can be inferred from different $^{208}\text{Pb}(d,p)^{209}\text{Pb}$ reaction data [32]. For the Maxwellian-averaged non-resonant DC cross section we obtained $\langle \sigma \rangle_{30\text{keV}}^{\text{DC}} = 0.135$ mb, which is in excellent agreement with experiment. The by far highest contributions to the DC cross section come from the E1 p -wave capture to the low spin states $J^\pi = 1/2^+, 3/2^+, 5/2^+$. Capture to the other states is negligible.

In order to test the different microscopic approaches we also calculated non-resonant DC on ^{208}Pb by consistently taking the input (energy levels, masses and nuclear densities) from the models described above. Again, the strength parameter λ of the folding potential in the entrance channel was adjusted to the elastic scattering data for each of the models. The calculations for the neutron capture cross sections yield 0.0289 mb, 0.0508 mb, and 0.0135 mb for RMFT, FRDM, and HFB, respectively. Hence, each of the models gives a smaller value for the Maxwellian-averaged 30 keV capture cross section than the calculation using experimental input data. The differences are due to the neutron separation energies and level schemes of the relevant states in ^{209}Pb (see Fig. 1) in the microscopic models, leading to different Q -values for capture to the excited states ($J^\pi = 1/2^+, 3/2^+, 5/2^+$). It should be noted that in Fig. 1 only those theoretical levels are shown which contribute to the cross section, i.e. only particle states. Capture into hole states is strongly suppressed by the fact that a re-ordering process would be required in the final nucleus (see e.g. [34] for a similar case). This would be reflected in extremely small spectroscopic factors. Therefore, the DC to such states is negligible.

V. RESULTS FOR NEUTRON-RICH PB ISOTOPES

We also investigated the model dependence of neutron capture on the neutron-rich even-even isotopes $^{210-238}\text{Pb}$. For these isotopes experimental data are only available near the region of stability. For more neutron-rich nuclei one has to rely solely on input parameters from microscopic models. In this and the following section we compare cross sections calculated with the nuclear properties predicted by different nuclear-structure models. Therefore,

we consider nuclear cross sections instead of Maxwellian-averaged ones as in the previous section.

Having obtained the relevant spins and calculated the Q -values from the masses as discussed above, we still had to determine the scattering potentials with their respective strength parameters (see Eq. 2). As a first step, the folding potentials were calculated, using the density distributions taken from the three different nuclear-structure models (HFB, RMFT, FRDM). In the potentials for each of the isotopes a factor λ was chosen giving the same volume integral as for the fitted $^{208}\text{Pb}+n$ potential, which was obtained as described in the previous section. This is justified because it is known that the volume integrals only change very slowly when adding neutrons to a nucleus [35]. For the bound state potentials λ is fixed by the requirement of correct reproduction of the binding energies. The spectroscopic factors were assumed to be unity for all transitions considered.

The results of our calculations are summarized in Fig. 2. For comparison, the levels from all of the models for ^{219}Pb , ^{229}Pb , and ^{239}Pb are shown in Figs. 3–5. The most striking feature in Fig. 2 is the sudden drop over several orders of magnitude in the cross sections calculated with the RMFT levels in the mass range $A = 212 - 220$. This is due to the lack of low spin levels which are cut off by the decreasing neutron separation energy. Only after the $1i_{11/2}$ orbital (which forms the state at lowest energy in the RMFT) has been filled completely at ^{222}Pb the cross section is increasing because low spin states become available again. A similar gap is seen for $A = 230 - 232$, and it is expected that those gaps will repeatedly appear when approaching the drip-line. Since in some cases there are unbound low spin states close to the threshold a small shift in the level energies could already close such a gap. However, note that the level spacing in the RMFT has the tendency to increase towards neutron rich nuclei [36], contrary to the FRDM and the HFB prediction.

The values resulting from the FRDM exhibit a smoother and almost constant behavior in the considered mass range. Only a slight dip is visible for $^{220}\text{Pb}(n,\gamma)$ since the previously accessible $1/2^+$ and $3/2^+$ states have become unbound in ^{221}Pb . The $2g_{9/2}$ orbital is at lower energy than the $11/2^+$ level in this model. Beyond ^{223}Pb it has been filled and at least one of the low spin states can be populated again. The known ground state spins for the lighter isotopes are also reproduced correctly. For higher mass numbers the cross sections are similar to the ones obtained in the HFB model.

For mass numbers below $A = 232$, the HFB capture cross sections are always larger than those obtained in the other models. Although the neutron separation energies are also decreasing, the Q -values for the capture to the low spin states become even larger, because the states are moving towards lower excitation energies. In general, the HFB cross sections of the investigated capture reactions exhibit a very smooth behavior with increasing neutron number.

VI. RESULTS FOR SN ISOTOPES

Proceeding in the same manner as for the Pb isotopes (Sec. V), we extended our investigation to the Sn nuclei. Here, the situation is different in two ways: Firstly, the drip-line lies at relatively much lower neutron numbers and the r-process path is not so far off stability, and secondly, there are more experimental data available also for the unstable nuclei close to or in the r-process path, which makes a test of theoretical models possible.

Again, we took the nuclear properties and density distributions from the above described models. The strengths of the scattering potentials were adjusted to reproduce the same value of the volume integral of 425 MeVfm^3 as determined from the experimental elastic scattering data on the stable Sn isotopes [7]. We calculated the capture cross sections from the stable isotope ^{124}Sn out to the r-process path which is predicted at a neutron separation energy of about 2 MeV [3]. As the models make different predictions about masses and separation energies, the r-process path is located at different mass numbers: $A \simeq 135$ for RMFT and FRDM and $A \simeq 145$ in the case of HFB. Contrary to the Pb isotopes for which the p -wave capture is the main contribution allowed by the electromagnetic selection rules, the Sn cross sections are dominated by the s -wave captures, due to the negative parities of the final states.

The level schemes of the ^{125}Sn , ^{133}Sn , and ^{141}Sn nuclei are shown in Figs. 6–8, and the resulting cross sections for all considered nuclei and models are combined in Fig. 9. Similarly as in the Pb case, the dependence of the cross sections on the mass number can be understood by considering the excitation energies of the low-spin states relative to the neutron separation energy predicted in various models (Figs. 10–12). The $3/2^-$ state is bound in the FRDM already at low mass number, whereas it becomes bound only at $A = 131$ and $A = 133$ in HFB and RMFT, respectively. Therefore, the FRDM cross sections are larger than the ones from HFB and RMFT for $A < 133$. The drop in the FRDM cross sections beyond the $N = 82$ shell is due to the fact that the $1/2^-$ and $3/2^-$ states slowly become unbound (see Fig. 12). In the HFB model the two low-spin states move down in energy faster than the neutron separation energy, thus providing an increasing Q -value and slightly increasing cross sections (Fig. 10). A similar trend can be found in the levels from RMFT, although with a less pronounced increase of the Q -value (Fig. 11).

There are no data available concerning the pure DC contribution to the cross sections for the neutron-rich Sn isotopes. However, there is experimental information regarding masses and level schemes. This can be compared to theory (see Fig. 7). For the experimentally known isotope ^{133}Sn we calculated DC by taking the experimentally known masses and levels [37] as input for the DC-calculation, thus arriving at a pseudo-experimental value for the cross section which can be compared to the purely theoretical predictions. The resulting value is marked by a cross in Fig. 9. Neutron capture on ^{132}Sn is particularly interesting because ^{133}Sn is predicted to be already very close to the r-process path by the two models RMFT and FRDM. As it turns out, however, the resulting cross sections show the closest agreement among the investigated nuclei for this case. All of the considered models predict the same ground state spin, a bound $3/2^-$ state and a (barely) unbound $1/2^-$ state (cf., Figs. 10–12, and Fig. 7; note that the mass ranges in the plots are different). However, the resulting Q -value is largest in the RMFT, yielding the highest cross section. The cross sections from the HFB and FRDM levels are smaller by about a factor of 2 because of the less strongly bound $3/2^-$ state. The additional $5/2^-$ state found in HFB gives only a small contribution to the total cross section and cannot compensate for the comparatively low Q -value of the capture to the $3/2^-$ level. Nevertheless, compared to the large discrepancies regarding other nuclei, there is good agreement in the resulting cross sections. Therefore, this nucleus may be a bad choice to select between the different models, but it is reassuring in the astrophysics context that the cross sections agree so well.

VII. DISCUSSION

In systematic r-process studies [3] it was found that the r-process path is touching nuclei with neutron separation energies around 2.5–1.7 MeV in the Sn region and $S_n \simeq 1.5 - 0.9$ MeV in the Pb region [3]. In our calculations for Pb (including $^{239}\text{Pb}+n$) we cover the astrophysically relevant mass region, with the possible exception of the HFB model. The neutron separation energies in the HFB model decrease much slower with increasing mass number than in the other models (cf., Fig. 5), thus not only leading to a drip-line at higher mass but also pushing the r-process path further out. However, the most extreme path location might still be further out by not more than two or three isotopes from ^{240}Pb , and therefore it is possible to extrapolate the trend seen in the HFB calculation at lower mass numbers. It should be kept in mind, however, that the location of the r-process path is determined by the ratio between neutron capture half-life and β -decay half-life.

In the following we briefly discuss the possible astrophysical consequences of the effects found in the cross section behavior given by the different models. Complete r-process network calculations, which take into account all possible reaction links and do not postulate an a-priori β -flow equilibrium, require a large number of astrophysical and nuclear-physics input parameters (for a detailed discussion, see e.g. [1]). In such a non-equilibrium scenario, the location of the r-process path as well as the time-scale of the r-matter flow is mainly determined by the neutron density as astrophysical quantity, and by the nuclear-physics parameters: the neutron separation energy S_n and the capture cross sections σ_n . With this, details of the r-process are depending on the specific nuclear models used. In the following discussion we will consider as a first estimate only the r-process paths found in detailed studies making use of FRDM masses [3] and vary the capture cross sections according to our findings for the different microscopic inputs.

In the mass region beyond the $A \simeq 195$ r-abundance peak, neutron densities of $n_n \simeq 10^{25} - 10^{27} \text{ cm}^{-3}$ are required to produce sizeable amounts of $Z \simeq 80 - 84$, $A \simeq 230 - 250$ r-process isotopes very far from β -stability. After successive β^- - and α -decays they will form the long-lived r-chronometers ^{232}Th and $^{235,238}\text{U}$, and the major part of the r-abundances of $^{206-208}\text{Pb}$ and ^{209}Bi (see, e.g. [38]). When regarding the σ_n cross sections for Pb from FRDM and HFB (see Fig. 2), very similar results are expected for the $^{230-238}\text{Pb}$ progenitor isotopes. Thus, also similar initial r-abundances for ^{232}Th and $^{235,238}\text{U}$ will result. However, when using the RMFT cross sections, a considerable hindrance of the nuclear flow around $A \simeq 130$ may occur which consequently would change the Th/U abundance ratios. These neutron capture cross sections which are 5 or more orders of magnitude smaller than the ones given by FRDM and HFB levels would increase the life-time of a nucleus against neutron-capture by the same order of magnitude and thus even prevent the flow to heavier elements within the time-scales given by the astrophysical environment.

In the case of the Sn isotopes, the situation is quite different from the Pb region. The range of astrophysically realistic n_n -conditions for producing the $A \simeq 130$ r-abundances is lower, with $n_n \simeq 10^{22} - 5 \times 10^{24} \text{ cm}^{-3}$. Hence, the r-process path is much closer to β -stability, involving the progenitor isotopes $^{134,136,138}\text{Sn}$ only a few neutrons beyond the doubly magic nucleus $^{132}_{50}\text{Sn}_{82}$. For these isotopes the Hauser-Feshbach (HF) cross sections used so far [1] are of the order of 10^{-4} to 5×10^{-5} barn. According to a recent investigation [13], the statistical model cannot be applied in that region and will overestimate the capture cross sections.

However, even if we use the experimental levels to calculate a Breit-Wigner resonant cross section for $^{132}\text{Sn}(n,\gamma)^{133}\text{Sn}$, we find it to be a factor of about 6 lower than the HF cross sections. Our present calculations would add another DC contribution of about the same magnitude as given by HF (see Fig. 9), which has so far not been taken into account. As a consequence of the larger total cross section, the r-matter flow to heavier elements would be facilitated, thus avoiding the formation of a pronounced $A \simeq 134 - 138$ “satellite peak” in the r-abundance curve sometimes observed in steady-flow calculations (see, e.g. Fig. 2 in [4], or Fig. 5 in [3]). Such a signature is only indicated in the heavy-mass wing of the $A \simeq 130$ $N_{r,\odot}$ -peak. It is interesting to note in this context that the HFB model, which exhibits the weakest $N = 82$ shell closure and with this also the weakest “bottle-neck” for the r-matter transit in this region (for a detailed discussion, see e.g. [39]), yields the highest DC cross sections for the $A \geq 134$ Sn isotopes.

Since we assumed spherical nuclei in order to be able to compare the different microscopic models, deformation effects were not taken into account which lead to level splitting and thus can increase the number of accessible levels. When considering deformation our results could be modified in two ways: Firstly, the number of bound low-spin levels could be increased, leading to larger DC cross sections; secondly, due to a possibly larger number of levels at and above the neutron separation energy, the compound reaction mechanism could be further enhanced and clearly dominate the resulting cross sections. However, as can be seen from level density [2,13] and deformation (e.g., [19]) studies, deformation of Pb isotopes sets in at a mass number of about $A \simeq 220$ and decreases already for masses beyond $A \simeq 230$. Closer to the drip-line, the nuclei show low level densities again, not only due to low neutron separation energies but also because of sphericity. Lead isotopes in the r-process path (especially for components with low S_n) will therefore already have reduced deformation and the DC – being sensitive to the level structure – will give an important contribution to the total capture cross sections. Concerning Sn, a theoretical study of the ratio of DC over CN contributions for Sn isotopes [7] shows that CN dominates up to a mass number $A \simeq 130$. Moreover, deformation is predicted to set in only at $A \simeq 140$ for Sn [20]. This is supported by level density considerations [13], showing that the level density is too low in this region to apply the statistical model. Therefore, depending on the model, the r-process path lies at the border of or already well inside the region where the DC is non-negligible and dominating.

Another source of uncertainty is the assumption of pure single-particle states, i.e., setting the spectroscopic factors to unity. This has been shown to be a good approximation for Pb isotopes close to stability and it is expected to hold for neutron-rich Pb isotopes. However, a range of 0.01–1.0 for the spectroscopic factors could be realistic. This will play only a minor role in the present comparison of different microscopic models, as the differences in the models may be only slightly enhanced when considering different theoretical spectroscopic factors. Nevertheless, it will be important in quantitative calculations of abundances, invoking complicated reaction networks.

VIII. SUMMARY

We have shown that theoretical capture cross sections can depend sensitively on the microscopic models utilized to determine the necessary input parameters. Because of low level

densities, the compound nucleus model will not be applicable in those cases. Drops over several orders of magnitude in the cross sections – as found with the RMFT for Pb – would change the position of the r-process path and possibly influence the formation of heavy chronometer elements, whereas the enhanced capture rates on Sn could have direct effects in the final r-process abundance distribution. Deformation effects and the compound nucleus reaction mechanism may still be of importance for the Pb isotopes and further investigations are needed. Nevertheless, the DC will be of major importance in the Sn region. This region is also interesting for future experimental investigations of S_n , neutron single-particle levels and (d,p)-reactions studying spectroscopic factors. There is also a need for improved microscopic nuclear-structure models which can also be compared in an astrophysical context following the successful tradition of the interplay between nuclear physics and astrophysics.

ACKNOWLEDGMENTS

This work was supported in part by the Austrian Science Foundation (project S7307–AST) and by the Polish Committee for Scientific Research. TR acknowledges support by an APART fellowship from the Austrian Academy of Sciences.

REFERENCES

- [1] J.J. Cowan, F.-K. Thielemann, and J.W. Truran, *Phys. Rep.* **208**, 267 (1991).
- [2] H. Oberhummer, H. Herndl, T. Rauscher, and H. Beer, *Surveys in Geophys.* **17**, 665 (1996).
- [3] F.-K. Thielemann, K.-L. Kratz, B. Pfeiffer, T. Rauscher, L. van Wormer, and M. Wiescher, *Nucl. Phys. A* **A570**, 329c (1995).
- [4] J. Chen, J. Dobaczewski, K.-L. Kratz, K.-H. Langanke, B. Pfeiffer, F.-K. Thielemann, and P. Vogel, *Phys. Lett. B* **355**, 37 (1995).
- [5] G.J. Mathews, A. Mengoni, F.-K. Thielemann, W.A. Fowler, *Ap. J.* **270**, 740 (1983).
- [6] S. Goriely, *Astron. Astrophys.* **325**, 414 (1997).
- [7] W. Balogh, R. Bieber, H. Oberhummer, T. Rauscher, K.-L. Kratz, P. Mohr, G. Staudt, and M.M. Sharma, in *Proc. Europ. Workshop on Heavy Element Nucleosynthesis*, eds. E. Somorjai and Z. Fülöp, Debrecen: Inst. Nucl. Res., 1994, p. 67.
- [8] K. Grün, R. Pichler, and H. Oberhummer, in *Neutrons and Their Applications*, eds. G. Vourvopoulos, T. Paradellis, *Proc. SPIE* 2339, 77 (1995).
- [9] J. Meißner, H. Schatz, J. Görres, H. Herndl, M. Wiescher, H. Beer, and F. Käppeler, *Phys. Rev. C* **53**, 459 (1996).
- [10] J. Meißner, H. Schatz, J. Görres, H. Herndl, M. Wiescher, H. Beer, and F. Käppeler, *Phys. Rev. C* **53**, 977 (1996).
- [11] H. Beer, P.V. Sedyshev, Yu.P. Popov, W. Balogh, H. Herndl, and H. Oberhummer, *Phys. Rev. C* **52**, 3342 (1995).
- [12] E. Krausmann, W. Balogh, H. Oberhummer, T. Rauscher, K.-L. Kratz, and W. Ziegert, *Phys. Rev. C* **53**, 496 (1996).
- [13] T. Rauscher, F.-K. Thielemann, and K.-L. Kratz, *Phys. Rev. C* **56**, 1613 (1997).
- [14] J. Dobaczewski, H. Flocard, and J. Treiner, *Nucl. Phys.* **A422**, 103 (1984).
- [15] J. Dobaczewski, I. Hamamoto, W. Nazarewicz, and J.A. Sheikh, *Phys. Rev. Lett.* **72**, 981 (1994).
- [16] M.M. Sharma, M.A. Nagarajan, and P. Ring, *Phys. Lett. B* **312**, 377 (1993).
- [17] M.M. Sharma, G.A. Lalazissis, and P. Ring, *Phys. Lett. B* **317**, 9 (1993).
- [18] P. Möller and J.R. Nix, *Nucl. Phys.* **A361**, 117 (1981).
- [19] P. Möller, J.R. Nix, W.D. Myers, and W.J. Swiatecki, *At. Data Nucl. Data Tables* **59**, 185 (1995).
- [20] P. Möller, J.R. Nix, and K.-L. Kratz, *At. Data Nucl. Data Tables* **66**, 131 (1997).
- [21] K.H. Kim, M.H. Park, and B.T. Kim, *Phys. Rev. C* **23**, 363 (1987).
- [22] K. Grün and H. Oberhummer, TU Wien, code TEDCA, 1995, unpublished.
- [23] A.M. Kobos, B.A. Brown, R. Lindsay, and G.R. Satchler, *Nucl. Phys.* **A425**, 205 (1984).
- [24] Y.K. Gambhir, P. Ring, and A. Thimet, *Ann. Phys. (NY)* **198**, 132 (1990).
- [25] H.C. Pradhan, Y. Nogami, and J. Law, *Nucl. Phys.* **A201**, 357 (1973).
- [26] P. Möller and J. Randrup, *Nucl. Phys.* **A514**, 1 (1990).
- [27] H. Beer, F. Corvi, and P. Mutti, *Ap. J.* **474**, 843 (1997).
- [28] R.L. Macklin, J. Halperin, and R.R. Winters, *Ap. J.* **217**, 222 (1977).
- [29] U. Ratzel, Forschungszentrum Karlsruhe (FZK), private communication.
- [30] H. de Vries, C.W. de Jager, and C. de Vries, *At. Data Nucl. Data Tables* **36**, 495 (1987).

- [31] G. Audi and A.H. Wapstra, Nucl. Phys. **A595**, 409 (1995).
- [32] M.J. Martin, Nucl. Data Sheets **63**, 723 (1991).
- [33] V.F. Sears, Neutron News **3**, 26 (1992).
- [34] T. Rauscher, W. Böhmer, K.-L. Kratz, W. Balogh, and H. Oberhummer, *Proc. ENAM 95*, eds. M. de Saint Simon, O. Sorlin (Editions Frontières, Gif-sur-Yvette 1995), p. 683.
- [35] G.R. Satchler, *Direct Nuclear Reactions* (Clarendon Press, Oxford, 1983).
- [36] M.M. Sharma, G.A. Lalazissis, W. Hillebrandt, and P. Ring, Phys. Rev. Lett. **72**, 1431 (1994).
- [37] P. Hoff, P. Baumann, A. Huck, A. Knipper, G. Walter, G. Marguier, B. Fogelberg, A. Lindroth, H. Mach, M. Sanchez-Vega, R.B.E. Taylor, P. van Duppen, A. Jokinen, M. Lindroos, M. Ramdhane, W. Kurcewicz, B. Jonson, G. Nyman, Y. Jading, K.-L. Kratz, A. Wöhr, G. Løvholden, T.F. Thorsteinsen, J. Blomqvist, and the ISOLDE collaboration, Phys. Rev. Lett. **77**, 1020 (1996).
- [38] B. Pfeiffer, K.-L. Kratz, and F.-K. Thielemann, Z. Phys. A **357**, 235 (1997).
- [39] K.-L. Kratz, B. Pfeiffer, and F.-K. Thielemann, *Proc. 6th Int. Conf. on Nucleus-Nucleus Collisions*, June 1997, Gatlinburg, TN, USA, in press.

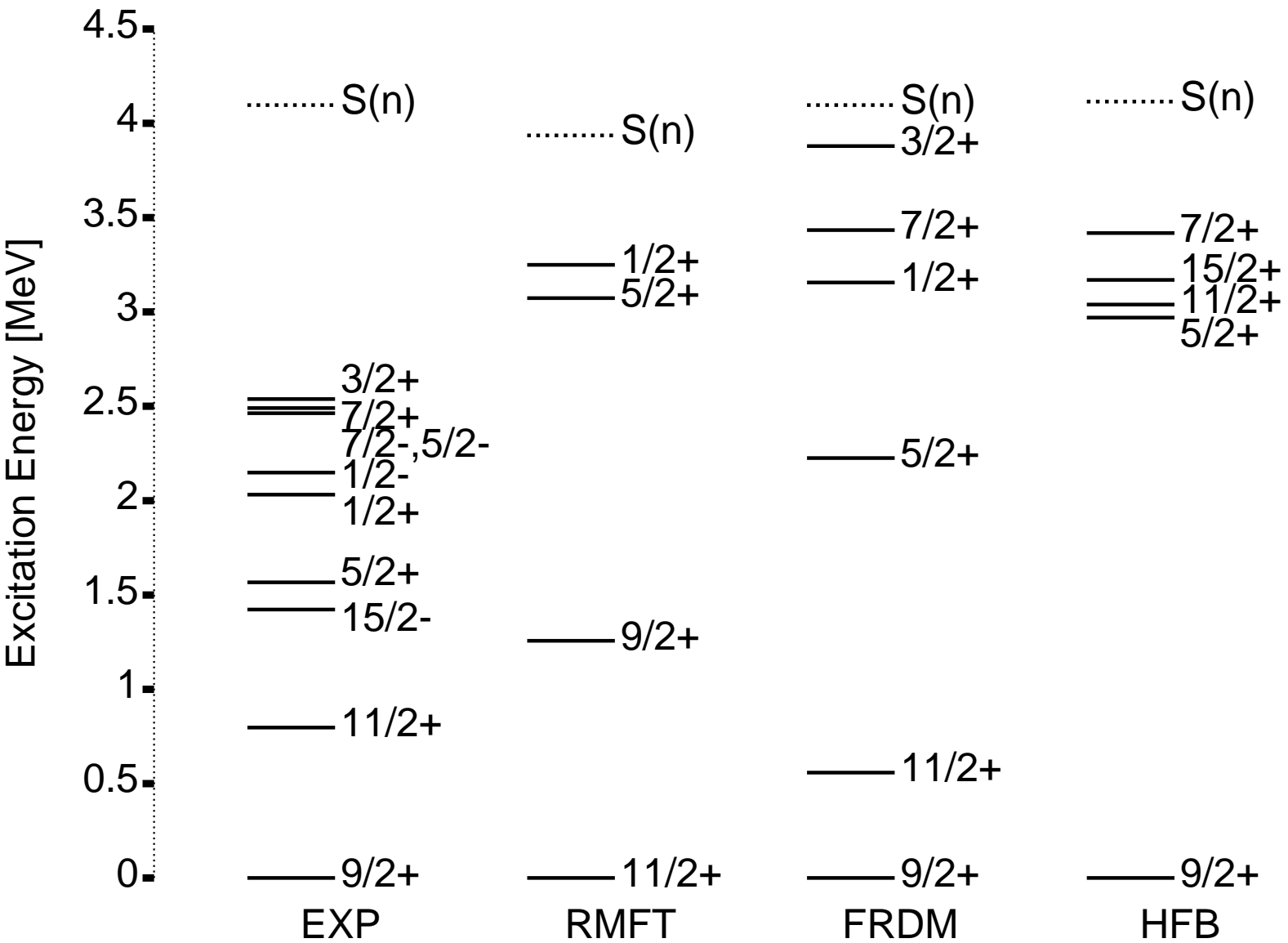


FIG. 1. Level schemes of ^{209}Pb obtained from experiment (EXP), and within the RMFT [17], FRDM [18], and HFB [14,15].

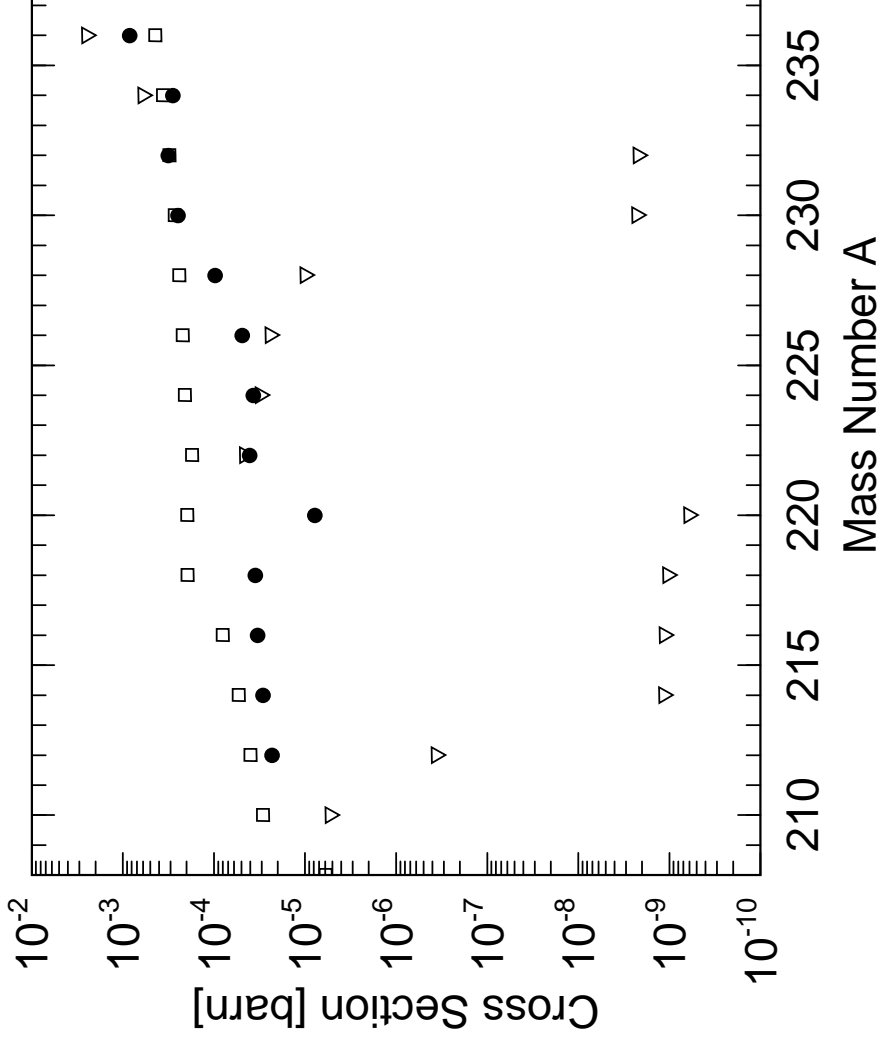


FIG. 2. Direct-capture cross sections at 30 keV for different Pb isotopes. Levels and masses are calculated within the RMFT (triangles), FRDM (dots), and HFB (squares).

FIG. 3. Level schemes of ^{219}Pb calculated within the RMFT, FRDM, and HFB.

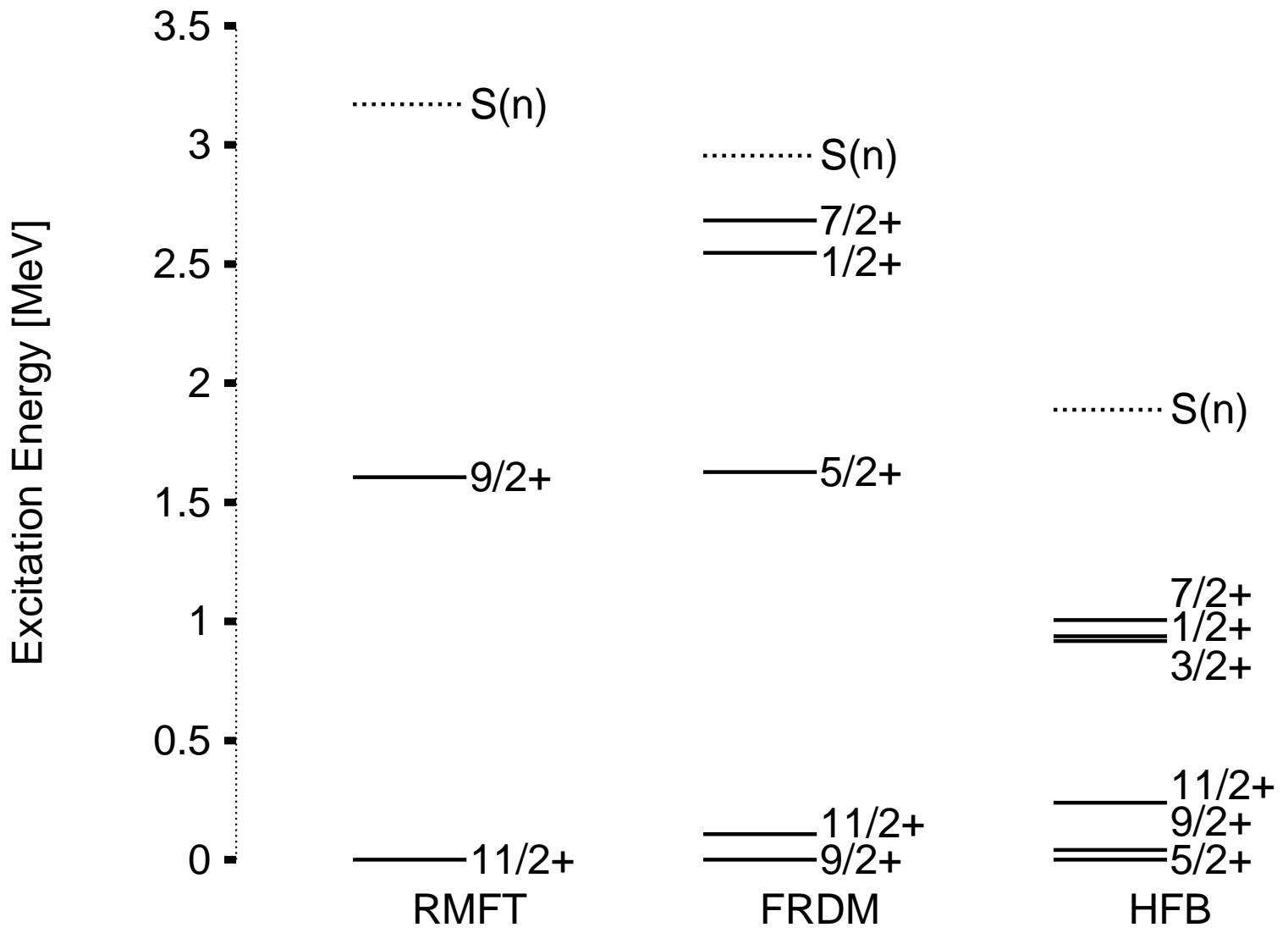
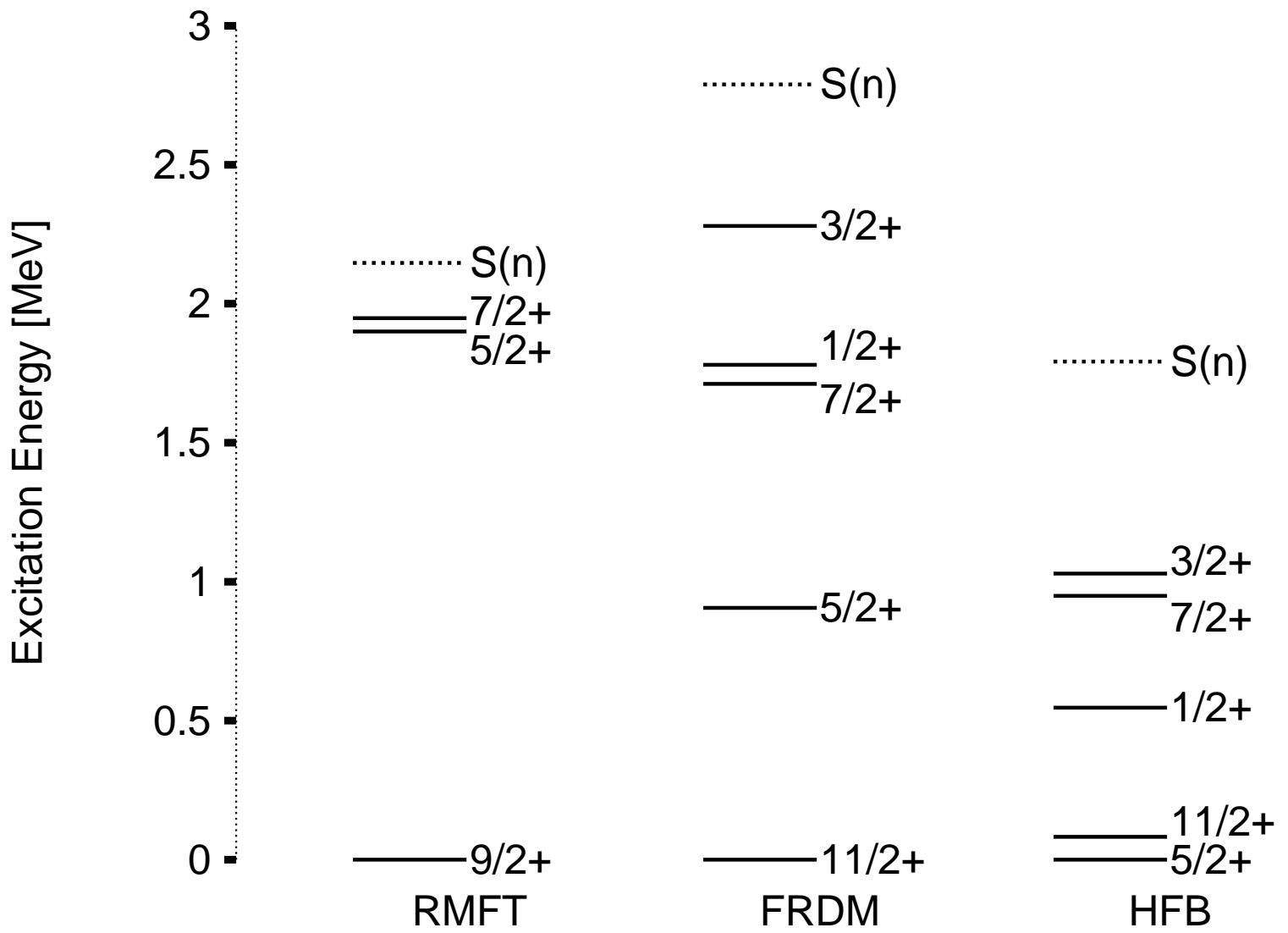


FIG. 4. Level schemes of ^{229}Pb calculated within the RMFT, FRDM, and HFB.



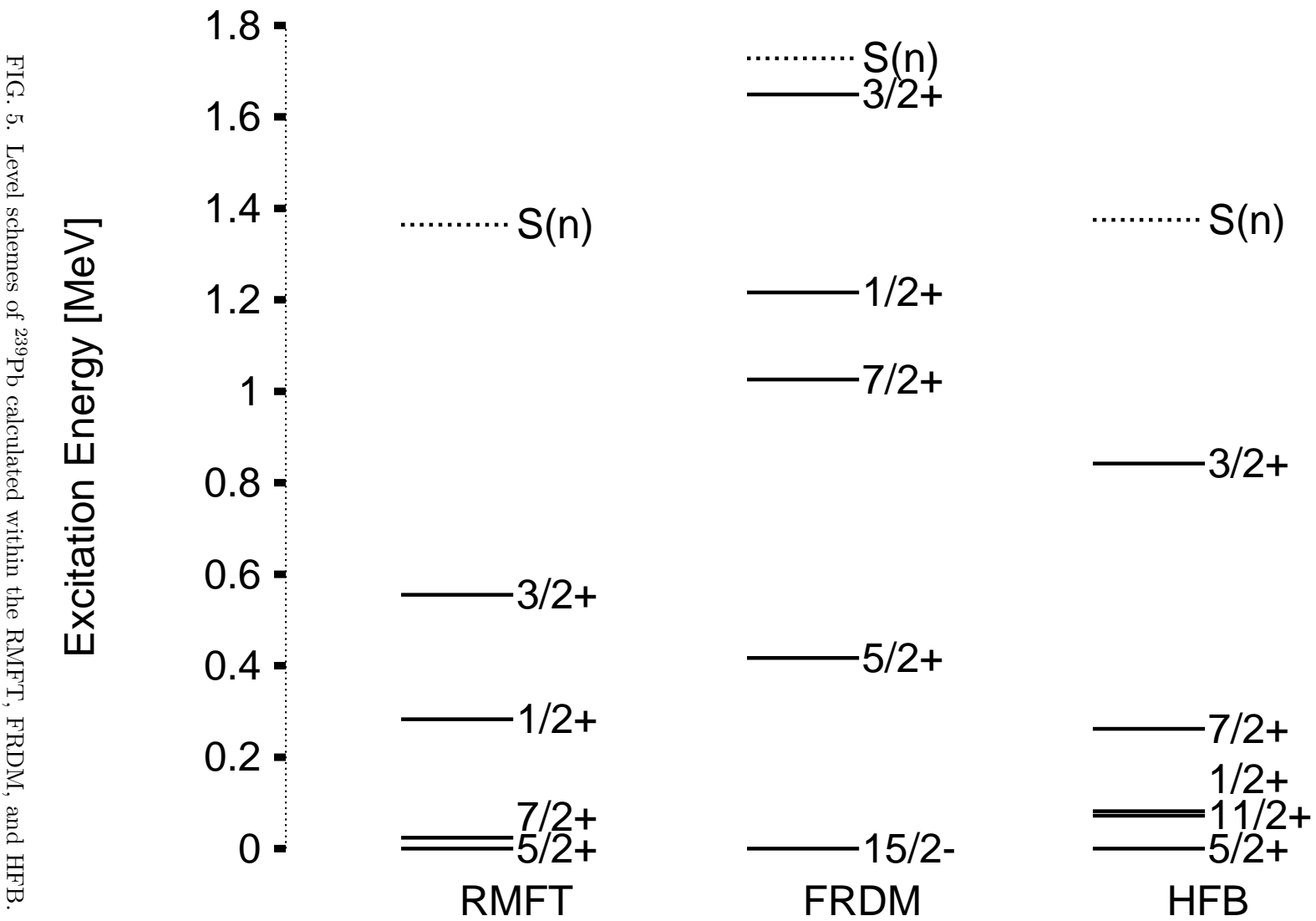
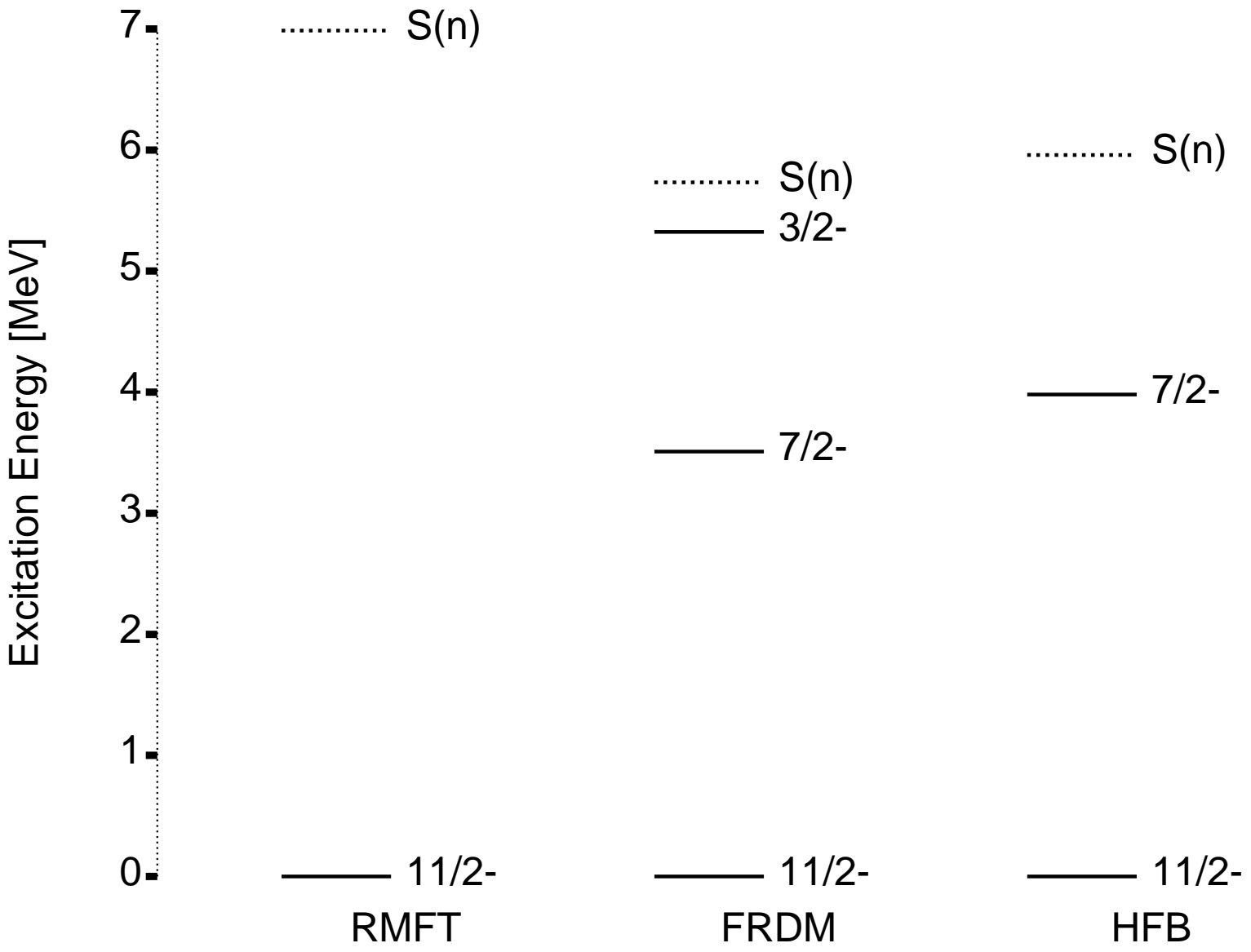


FIG. 5. Level schemes of ^{239}Pb calculated within the RMFT, FRDM, and HFB.

FIG. 6. Level schemes of ^{125}Sn calculated within the RMFT, FRDM, and HFB.



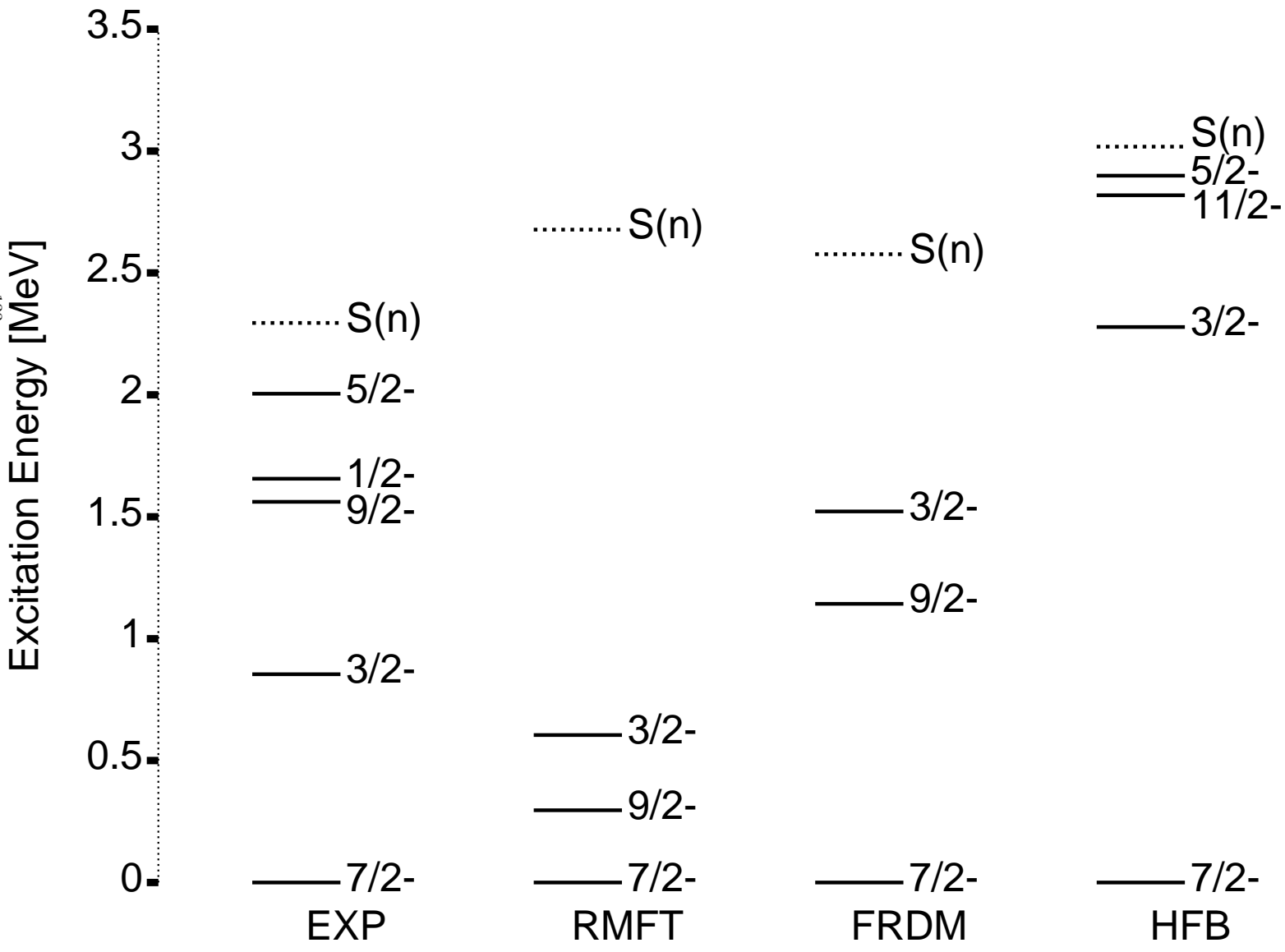


FIG. 7. Level schemes of ^{133}Sn calculated within the RMFT, FRDM, and HFB. Experimental levels are taken from Ref. [37].

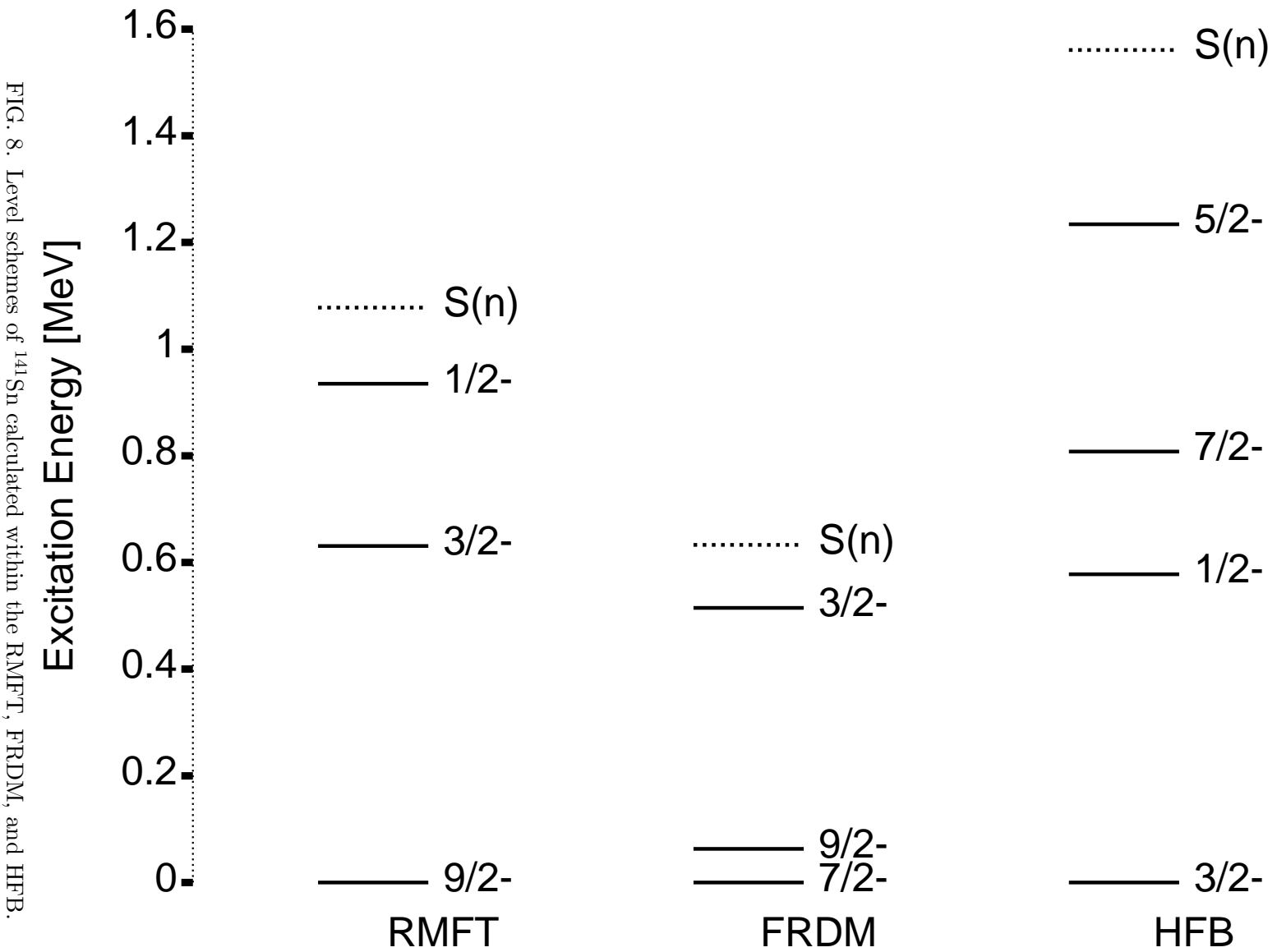


FIG. 8. Level schemes of ^{141}Sn calculated within the RMFT, FRDM, and HFB.

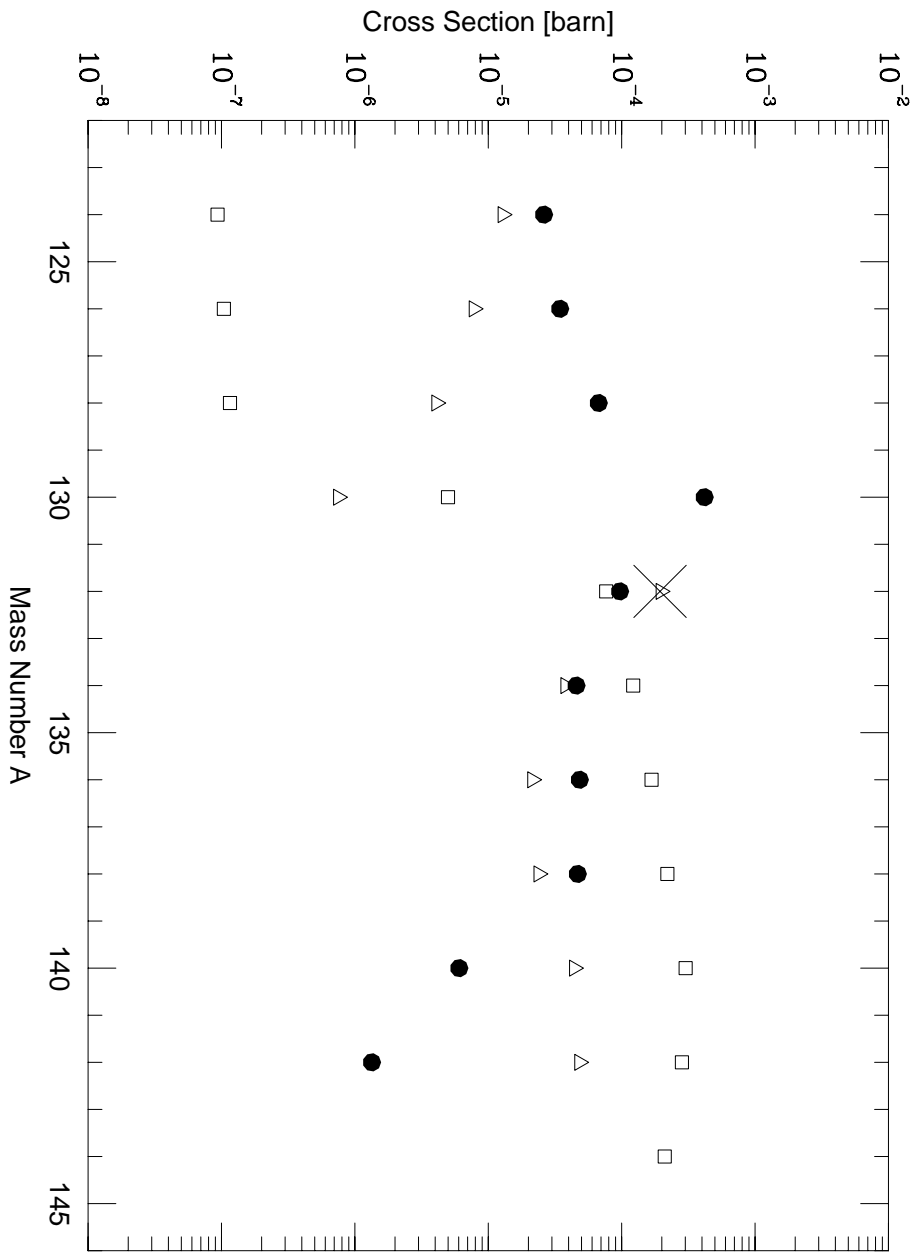


FIG. 9. Same as in Fig. 2 but for the Sn isotopes. The cross section resulting from a calculation using experimental levels [37] is marked by a cross.

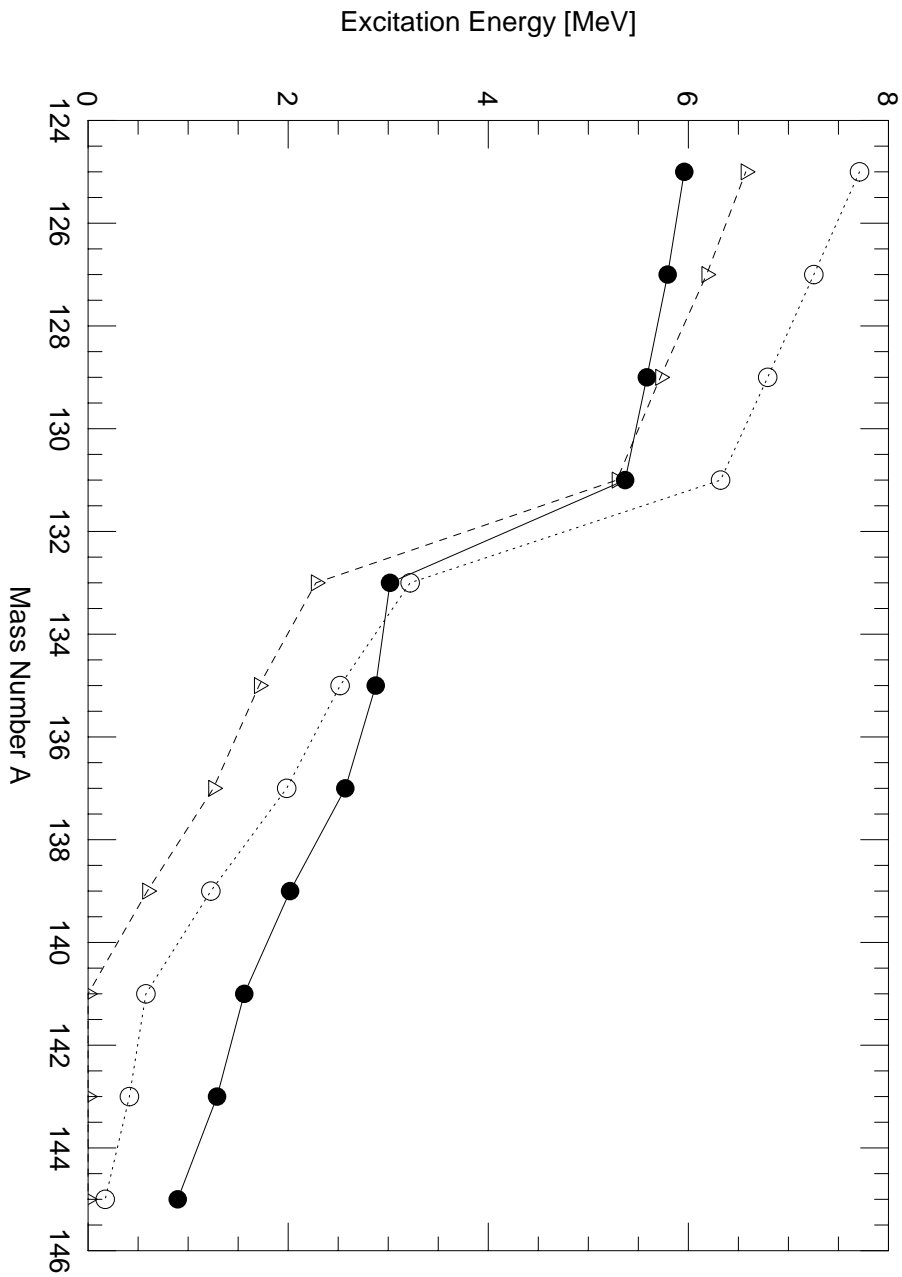


FIG. 10. Dependence of level energies on mass number for the even-odd Sn isotopes calculated in the HFB model. Shown are the $1/2^-$ state (open circles), the $3/2^-$ state (triangles) and the calculated neutron separation energy (full circles). The lines are drawn to guide the eye.

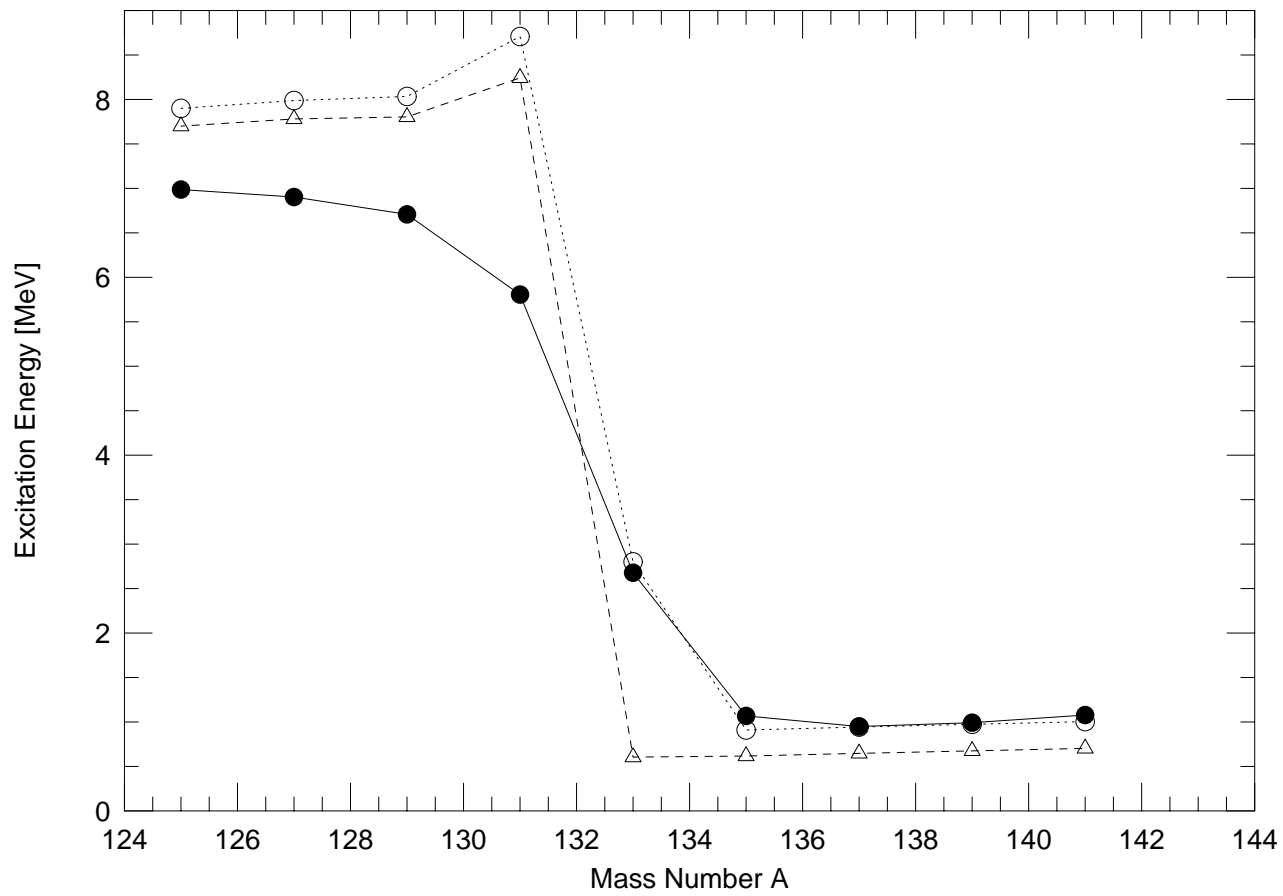


FIG. 11. Same as in Fig. 10 but for the RMFT.

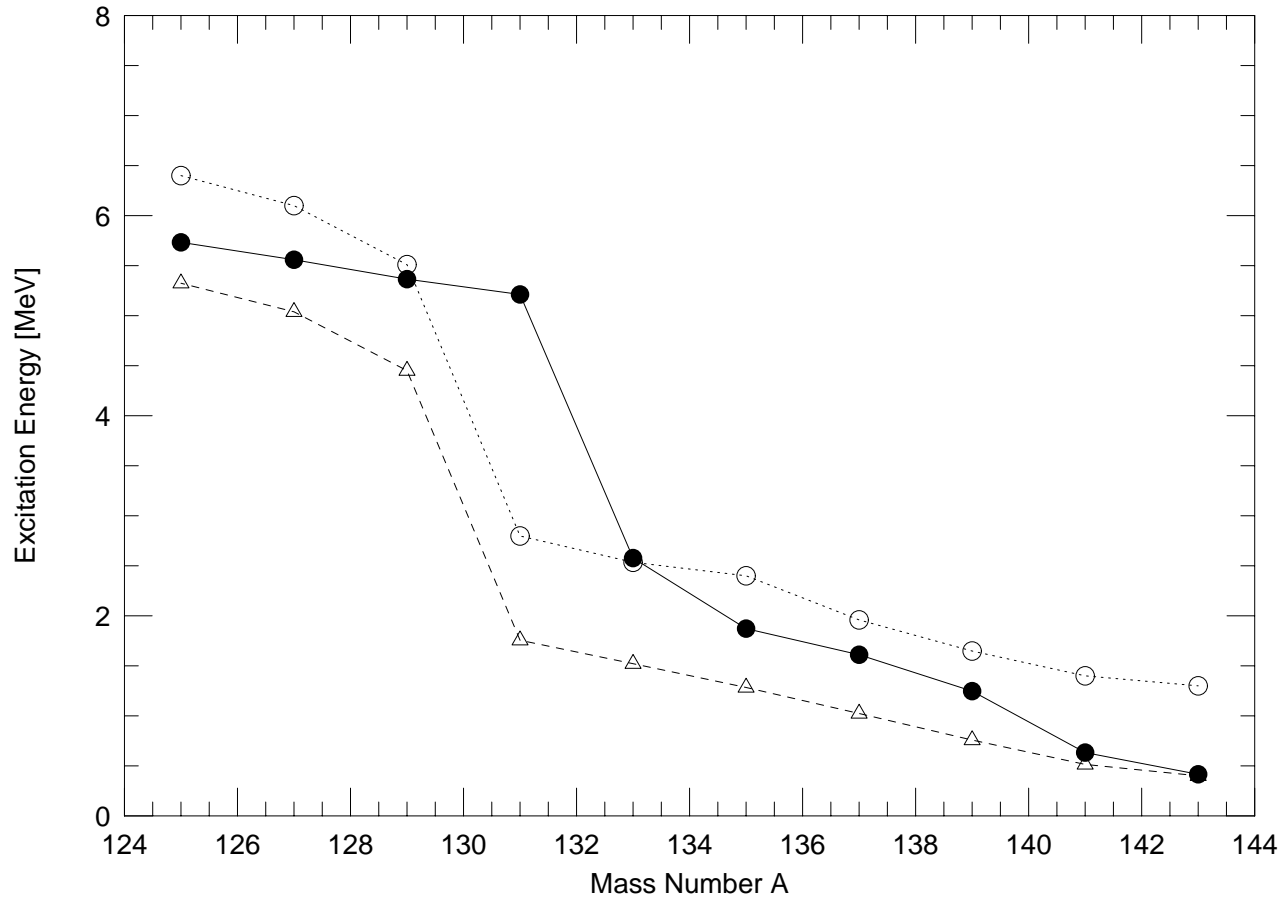


FIG. 12. Same as in Fig. 10 but for FRDM levels.